POLITECNICO DI TORINO
Repository ISTITUZIONALE

Modeling Infrared Superlattice Photodetectors: From Nonequilibrium Green's Functions to Quantum-Corrected Drift Diffusion

Original
Modeling Infrared Superlattice Photodetectors: From Nonequilibrium Green's Functions to Quantum-Corrected Drift Diffusion / Tibaldi, A., GONZALEZ MONTOYA, J.A., Vallone, M.E., Goano, M., Bellotti, E., Bertazzi, F.. - In: PHYSICAL REVIEW APPLIED. - ISSN 2331-7019. - STAMPA. - 16:4(2021), p. 044024. [10.1103/PhysRevApplied.16.044024]

Availability:
This version is available at: 11583/2931830 since: 2021-10-15T13:37:38Z

Publisher:
American Physical Society

Published
DOI:10.1103/PhysRevApplied.16.044024

Terms of use:

This article is made available under terms and conditions as specified in the corresponding bibliographic description in the repository

Publisher copyright

(Article begins on next page)

29 November 2026

Modeling Infrared Superlattice Photodetectors: From Nonequilibrium Green's Functions to Quantum-Corrected Drift Diffusion

Alberto Tibaldi,[1,2,*] Jesus Alberto Gonzalez Montoya,[1] Marco Vallone,[1] Michele Goano,[1,2] Enrico Bellotti,[3] and Francesco Bertazzi[1,2]

[1] *DET, Politecnico di Torino, Torino, Italy*

[2] *IEIIT-CNR, Torino, Italy*

[3] *Department of Electrical and Computer Engineering, Boston University, Boston, Massachusetts 02215, USA*

(Received 4 June 2021; revised 19 August 2021; accepted 24 September 2021; published 14 October 2021)

Carrier transport in type-II superlattice photodetectors is investigated by means of a rigorous nonequilibrium Green's function model based on a physics-based Büttiker-probe formalism. Intraband scattering self-energies (carrier-phonon interactions) are computed in the self-consistent Born approximation, while interband self-energies (Shockley-Read-Hall and optical transitions) are included in terms of semiclassical generation-recombination rates, neglecting interband renormalization effects. Current conservation is achieved with an efficient Newton-Raphson algorithm. While carrier transport in infrared detectors is usually understood in terms of quantities (e.g., mobilities and quasi-Fermi-levels) that are admittedly not germane to nonequilibrium Green's function theory, the proposed model provides a quantum-kinetic description of tunneling, miniband transport, hopping, and carrier extraction within a drift-diffusion-friendly framework. The connection with semiclassical theories allows exploration of the possibilities offered by Poisson-Schrödinger or localization landscape drift-diffusion approaches.

DOI: 10.1103/PhysRevApplied.16.044024

I. INTRODUCTION

Some specific properties of type-II superlattices (T2SLs), in particular, the splitting of the HH1 and LH1 sub-bands and the characteristics of the evanescent states connecting the (propagating) valence- and conduction-band states, hold the promise of an ideal absorbing material with small Auger recombination coefficients and reduced band-to-band tunneling at arbitrarily small band gaps [1]. Motivated by these favorable theoretical predictions, antimonide-based T2SLs were proposed as a possible alternative to the well-established infrared detector technology based on mercury cadmium telluride ($Hg_{1-x}Cd_xTe$), with the additional potential advantage of the competitive costs afforded by the standard III-V growth technology. As type-II infrared detectors are now approaching, but still not outperforming the dark current characteristics of state-of-the-art $Hg_{1-x}Cd_xTe$ detectors, at least in the long-wavelength infrared region, gradually emerging is the question whether the performance of T2SL detectors is ultimately limited by the presence of extrinsic recombination centers, or by intrinsic carrier-transport properties, which could be possibly improved by proper superlattice design.

The most striking aspect of T2SL photodetectors is perhaps the extreme diversity of the possible carrier-transport mechanisms, which range from miniband transport to Wannier-Stark hopping, depending on geometrical parameters, temperature, and the presence of built-in and/or applied fields [2]. Particularly in the long-wavelength infrared (LWIR) spectral region, the hole miniband is typically very narrow compared to the electron miniband. Therefore, vertical electron transport appears phonon-scattering-limited, which is indicative of miniband transport, while vertical hole transport is best described by hopping between localized states mediated by electron-phonon coupling, with transport being favored by scattering, rather than inhibited. The hole mobility may be significantly reduced in the presence of disorder, while electron transport is much less sensitive to the presence of defects. Indeed, the very concept of miniband conduction breaks down when the miniband width is very small, as growth imperfections may completely disrupt the alignment of the energy levels in the weakly coupled limit [3].

It is generally understood that native defects associated with GaSb are responsible for the SRH-limited minority-carrier lifetimes observed in InAs/GaSb T2SLs, while gallium-free InAs/$InAs_{1-x}Sb_x$ superlattices exhibit much longer lifetimes, comparable with those obtained in $Hg_{1-x}Cd_xTe$ alloys, but a longer superlattice period is needed to achieve long wavelength cutoffs, which results

*alberto.tibaldi@polito.it

 © 2021 American Physical Society

in reduced vertical hole mobilities and weaker absorption coefficients [4].

Although approximations may apply in specific cases, a general theory is needed whenever the miniband width, the scattering-induced broadening, and the potential drop per period take similar values [2]. This is the most likely scenario in type-II superlattice detectors, where there is generally a coexistence of localized states acting as trap centers, and miniband states sufficiently extended to allow transport above the mobility edge [5]. Based on a self-consistent description of electronic structure and scattering processes—in which the broadening of the states emerges naturally—the nonequilibrium Green's function (NEGF) approach seamlessly describes the transition between these transport regimes. However, the staggering computational cost required by the calculation of Green's functions, especially in the multiband case, limits the NEGF analysis to very simple structures [3]. These considerations strongly prompt towards exploring the possibilities offered by simplified NEGF models based on the effective mass approximation, or even quantum-corrected semiclassical approaches based on the well-established numerical framework of the basic drift-diffusion (DD) model, which has been successfully employed for the calculation of the relevant figures of merit (quantum efficiency, crosstalk, and modulation transfer functions) of bulk $Hg_{1-x}Cd_xTe$ detectors [6].

Among possible quantum-corrected semiclassical approaches [7–11], the Schrödinger-Poisson drift-diffusion model (SPDD) represents a natural extension of the classical DD framework. Quantum effects are incorporated by means of a modified local density of states (LDOS) [8] derived from the Schrödinger equation, while the scattering mechanisms are still phenomenologically encoded in appropriate mobility models. Recent advances in the calculation of the LDOS from the localization landscape theory [12,13] make such quantum-corrected DD approaches promising for three-dimensional device simulation. Notable carrier transport studies inspired by Anderson localization theory [14] have been presented in the context of T2SL $InAs/InAs_{1-x}Sb_x$ photoconductors [15], and nitride-based light-emitting diodes (LEDs) [16]. It should be mentioned, however, that the localization-landscape (LL) theory was originally proposed to study the ground-state properties of disordered systems. As the landscape paradigm was just recently shifted to the analysis of carrier-transport properties, many aspects of this interesting development need to be clarified. For example, in a superlattice, one may expect that tunneling currents caused by the tail states in the barrier layers should be somehow included in the lowering of the effective potential, but a quantitative assessment of this intuition is still missing.

A recent study of carrier transport in GaN-based LEDs has reported a quantitative agreement between NEGF calculations based on the Büttiker probe formalism and quantum-corrected DD simulations [17], save for situations with pronounced tunneling and interference effects. The discrepancies between NEGF and semiclassical models, which appear when the density of states is strongly modified with respect to the bulk case, were attributed to the somewhat arbitrary distinction between carriers populating bound and unbound states, which is implicit in any DD model that attempts to solve the dynamics of the two populations coupled by rate equations [17], and to the use of phenomenological Büttiker probe self-energies, whose expression does not depend on Green's functions [17]. Since we are concerned with carrier transport in a superlattice, where the transport itself is made possible by the formation of minibands, we propose a DD-friendly, yet rigorous NEGF model based on a physics-based formulation of the Büttiker probe self-energies, extending the work in Ref. [17] to T2SLs. The model is applied to *n*B*n* detectors, which are essentially a photodiode with the junction (space-charge region) replaced by an electron blocking unipolar barrier (B), and the *p*-type contact replaced by an *n*-type contact, see Ref. [18] for a classification of barrier detectors. As a preliminary step towards the development of a library of material parameters for the most common T2SL configurations, we compare the NEGF simulations with a quantum-corrected SPDD model based on the full eigendecomposition of the Schrödinger equation. In the spirit of LL approaches, no distinction is made between localized and delocalized states in SPDD, which enables a more fair comparison with NEGF results.

II. THEORY

We assume a single-band effective-mass Hamiltonian for one-dimensional slab systems (to simplify the notation, we write only the equations corresponding to electron transport, the extension to the bipolar case being straightforward)

$$H(z,k_t) = -\partial_z \frac{\hbar^2}{2m^*_{e,z}} \partial_z + E_C(z) + \frac{\hbar^2 k_t^2}{2m^*_{e,t}}, \tag{1}$$

where $m^*_{e,t}$, $m^*_{e,z}$ are electron effective masses along the in-plane and growth directions, respectively, and E_C is the conduction-band edge. We also assume that retarded components of Green's functions and self-energies depend only on the energy E and the norm of the in-plane wave vector k_t ($O = G, \Sigma$) [19]

$$O^R(k_t, z, z'; E) = O^R(z, z'; E - E_{k_t}). \tag{2}$$

The quantum-kinetic version of the DD equations, i.e., the continuity equation expressing charge conservation, complemented with the Poisson equation accounting for electron-electron interactions at the Hartree level,

reads [20]

$$\partial_z^2\phi(z) = -\frac{e}{\varepsilon}\left[N_D(z) - N_A(z) + p(z) - n(z)\right], \tag{3}$$

$$\partial_z J_n(z) = e\, U_n(z), \tag{4}$$

$$n(z) = -i\int \frac{dE}{2\pi} G^<(z,z,E), \tag{5}$$

$$J_n(z) = \lim_{z'\to z}\frac{e\hbar}{m_0}(\partial_z - \partial_{z'})\int \frac{dE}{2\pi} G^<(z,z',E), \tag{6}$$

where e is the elementary charge, ε is the dielectric constant, N_D, N_A are the donor and acceptor densities, n and p are the electron and hole densities, m_0 is the bare electron mass, and U_n is the (net) recombination rate

$$\begin{aligned} U_n(z) = -\frac{2}{\hbar}\int \frac{dE}{2\pi}\int dz' \big[&\Sigma^R(z,z',E)G^<(z',z,E) \\ &+ \Sigma^<(z,z',E)G^A(z',z,E) \\ &- G^R(z,z',E)\Sigma^<(z',z,E) \\ &- G^<(z,z',E)\Sigma^A(z',z,E)\big]. \end{aligned} \tag{7}$$

A full implementation of carrier transport requires the self-consistent solution of the Dyson equation and Keldysh equations

$$\begin{aligned} G^R(z,z',E) = G_0^R(z,z',E) + \int dz_1 \int dz_2 \\ \times G_0^R(z,z_1,E)\Sigma^R(z_1,z_2,E)G^A(z_2,z',E) \end{aligned} \tag{8}$$

$$\begin{aligned} G^<(z,z',E) = \int dz_1 \int dz_2\, G^R(z,z_1,E) \\ \times \Sigma^<(z_1,z_2,E)G^A(z_2,z',E), \end{aligned} \tag{9}$$

where G_0^R is Green's function of the noninteracting system. The retarded Green's function gives the excitation spectrum of the nanostructure and is related to the LDOS, the lesser Green's function describes how the states are occupied and determines the relevant one-particle properties, such as charge and current densities. The independent evaluation of the density of states and their occupation violates Pauli blocking [21]. The coupling of the Dyson and Keldysh equations is indeed one of the most demanding features of the NEGF formalism [21]. The Büttiker probes were originally proposed as a phenomenological model to provide a simplified description of the relevant (intraband) self-energies, e.g., electron-electron and electron-phonon scattering, which are usually obtained within the self-consistent Born approximation through a fixed-point iterative solution of the NEGF equations [22–24]. Within the Büttiker formalism, current conservation is achieved by simply adjusting the position-dependent Fermi levels of the probes using a fast converging Newton-Raphson algorithm. But the numerical and conceptual simplicity of the Büttiker probes does not limit their application to phenomenological and oversimplified dissipation models, as was shown in the context of quantum cascade lasers [19]. Recently, carrier-phonon self-energies compatible with the Büttiker-probe formalism were employed in atomistic simulation of graphene nanotransistors [25]. Following Ref. [25], deformation potential scattering assisted by acoustic and optical phonons results in a (local) intraband self-energy compatible with ansatz (2)

$$\begin{aligned} \Sigma^R_{\mathrm{BP}}(z,z,E) = \frac{\hbar D_A^2 k_B T}{\rho v_l a}\, G^R(z,z,E) + \frac{\hbar D_{tK}^2}{2\rho\omega_0 a} \\ \times \left\{\left[n_0 - f\left(E - E_0 - E_{\mathrm{BP}}^{(\mathrm{n})}\right) + 1\right]\right. \\ \times G^R(z,z,E-E_0) \\ + \left[n_0 + f\left(E + E_0 - E_{\mathrm{BP}}^{(\mathrm{n})}\right)\right] \\ \left.\times\, G^R(z,z,E+E_0)\right\}, \end{aligned} \tag{10}$$

where f is the Fermi-Dirac function, $E_{\mathrm{BP}}^{(n)}(z)$ is the position-dependent Fermi level of the Büttiker probes in the conduction band, D_A, D_{tK} are the acoustic and optical deformation potentials, respectively, ρ is the density of the material, v_l is the longitudinal sound velocity, $E_0 = \hbar\omega_0$ is the energy of optical phonons, n_0 is the number of optical phonons, and a is the lattice constant.

In principle, polar optical scattering should be included as an additional self-energy, but the momentum dependence of the Fröhlich scattering potential would not be compatible with the implicit summation over transverse wave vectors granted by ansatz (2). Moreover, the spatial nonlocality that originates from the long-range nature of the Coulomb potential cannot be described within the Büttiker-probe formalism, which implicitly assumes diagonal self-energies. A common approximation in the analysis of quantum cascade lasers is to ignore the momentum dependence of the self-energies, e.g., by evaluating the matrix elements at typical in-plane momenta [26]. This approximation gives accurate results when typical momentum transfers are chosen carefully [27], although the energy dependence of the scattering processes is not represented correctly [21,28]. The underestimation of the carrier-phonon coupling strength in local scattering models [29] can be approximately corrected by multiplying the self-energies by a compensation factor obtained from Fermi's golden rule [30]. Neglecting nonlocal effects and momentum dependence, the polar optical self-energy takes the same form of the optical deformation potential self-energy [19], which allows us to consider D_{tK} as an effective parameter that comprehensively describes inelastic carrier-phonon interactions, both polar and not, within the approximations discussed above. The numerical values of D_{tK} and

TABLE I. List of simulation parameters.

Quantity	Value
D_A	8 eV
D_{tK}	1×10^9 eV/cm
ρ	5.32 g/cm^3
v_l	6.56 km/s
E_0	30 meV
$m^*_{e,t}$	0.045 m_0
$m^*_{e,z}$	0.035 m_0
$m^*_{h,t}$	0.05 m_0
$m^*_{h,z}$	0.28 m_0

other parameters employed in the simulations are reported in Table I.

The lesser component of the Büttiker self-energy is

$$\Sigma^<_{\mathrm{BP}}(z,z,E) = i\frac{m^*_{e,t}}{\pi\hbar^2}k_BT\,\mathcal{F}_0\left(\frac{E-E^{(\mathrm{n})}_{\mathrm{BP}}}{k_BT}\right)\Gamma_{\mathrm{BP}}(z,z,E) \tag{11}$$

with the broadening function

$$\Gamma_{\mathrm{BP}}(z,z,E) = i\left[\Sigma^R_{\mathrm{BP}}(z,z,E) - \Sigma^A_{\mathrm{BP}}(z,z,E)\right]. \tag{12}$$

The sum over transverse wave vectors, necessary for the calculation of the observables, has been carried out by replacing in Eq. (11) the Fermi-Dirac function f with the zero-order incomplete Fermi-Dirac integral $\mathcal{F}_0$ [31,32].

Turning our attention to the continuity equation, Eq. (4), the additive property of the self-energies in Eq. (7), allows the decomposition of U_n in the sum of different scattering processes. Upon convergence, the contribution of intraband mechanisms (the interaction with phonons) should vanish when the integral over energy is performed over one of the two (conduction or valence) bands. Interband scattering processes, e.g., optical and Shockley-Read-Hall (SRH) transitions, connecting the conduction and valence bands, can be treated within the NEGF formalism on equal footing with inelastic quantum transport [33], but in the spirit of the drift-diffusion approximation, we neglect interband renormalization effects by computing U_n with semiclassical expressions [17,34]. In order to investigate the extraction efficiency of T2SL detectors, we assume $U_n = U_{\mathrm{SRH}} - G_{\mathrm{opt}}$, where G_{opt} is a constant optical generation rate computed from the absorption in the material and the photon flux, and U_{SRH} is the (net) SRH recombination rate given by

$$U_{\mathrm{SRH}}(z) = \frac{np - n_{\mathrm{eq}}p_{\mathrm{eq}}}{\tau_p(n+n_1)+\tau_n(p+p_1)}, \tag{13}$$

where n_{eq}, p_{eq} are the electron and hole densities at equilibrium, and n_1, p_1 are the corresponding quantities when the Fermi level falls at the trap energy level.

Representing carrier states in a finite-element basis, the NEGF version of the continuity equation, Eq. (4), reads in full matrix notation

$$\frac{e}{\hbar}\int\frac{dE}{2\pi}\,\mathrm{Tr}\{hG^<(E) - G^<(E)h\} = eU_n, \tag{14}$$

where $h = EM - H$, M is the overlap matrix, and the trace is performed over finite-element degrees of freedom. A simple iteration scheme between Green's functions and self-energies in the self-consistent Born approximation may take several thousands of iterations to converge, depending on the localization of the states [29]. On the other hand, a Newton-Raphson algorithm may achieve convergence in just few iterations. Among the advantages of the Büttiker formalism is the possibility to compute the Jacobian matrix analytically. Usually, the Poisson equation is solved in a separate (outer) self-consistent loop, but we prefer to find the self-consistent electrostatic (Hartree) potential and Fermi levels within a single Newton iteration scheme, exactly as in a DD model, using the identity

$$\partial_\phi G^R = -G^R\partial_\phi(h - \Sigma^R)G^R, \tag{15}$$

to compute the derivative of the retarded Green's function with respect to the potential ϕ. Boundary conditions are enforced by fixing the unknowns $E^{(n)}_{\mathrm{BP}}$, and ϕ in additional superlattice layers on both sides of the contact regions.

Formally, the Fermi levels of the Büttiker probes coincide with the Fermi levels only at equilibrium, where the fluctuation-dissipation theorem applies. However, if we invoke the concept of quasiequilibrium, it makes sense to compare the Fermi levels of the probes with the quasi-Fermi-levels obtained with a quantum-corrected DD model.

A. Schrödinger-Poisson drift diffusion

The SPDD model, includes quantum corrections to the electrostatics by means of a modified LDOS. In steady-state conditions, the model equations read (for shortness we write only the equations for electrons)

$$\partial_z^2\phi(z) = -\frac{e}{\varepsilon}\left[N_D(z) - N_A(z) + p(z) - n(z)\right], \tag{16}$$

$$\partial_z J_n(z) = e\,U_n(z), \tag{17}$$

$$J_n(z) = e\mu_e n\partial_z\left(\tilde{E}_{\mathrm{C}} + k_BT\log N_C + k_BT\log\gamma_n\right) \tag{18}$$

$$-\partial_z\frac{\hbar}{2m^*_{e,z}}\partial_z\psi_n(z) + E_C(z)\psi_n(z) = E\psi_n(z), \tag{19}$$

where

$$\gamma_n = \frac{\mathcal{F}_{1/2}\left(\dfrac{E_F^{(n)} - \tilde{E}_C}{k_B T}\right)}{\exp\left(\dfrac{E_F^{(n)} - \tilde{E}_C}{k_B T}\right)} \tag{20}$$

accounts for Fermi-Dirac statistics [35]. The electron charge is computed as

$$n(z) = \frac{m^*_{e,t}}{2\pi\hbar^2} \sum_i |\psi_n^{(i)}(z)|^2 \mathcal{F}_0\left(\frac{E_i - E_F^{(n)}}{k_B T}\right), \tag{21}$$

$E_C = -e\phi + \Delta E_C$ is the conduction-band edge, while the effective conduction-band edge $\tilde{E}_C$ is obtained from

$$n(z) = N_C \mathcal{F}_{1/2}\left(\frac{E_F^{(n)} - \tilde{E}_C}{k_B T}\right), \tag{22}$$

where N_C is the three-dimensional effective density of states. The quantum-corrected DD formulation presented here is equivalent to the approach proposed in Ref. [8], in which the quantum corrections have been included in γ_n. SPDD shares the same idea of the LL approach, in particular, the definition of an equivalent semiclassical confining potential seen by the carriers, with the only difference that the quantum electron density is not approximated by a landscape equation, but it is obtained directly from the full eigendecomposition of the Schrödinger equation, Eq. (19). While the SPDD approach may not be viable in three-dimensional simulations, it provides a benchmark for the accuracy of LLDD models.

III. RESULTS

Among possible candidates for the assessment of the sophisticated physics in T2SLs, barrier infrared detectors provide the opportunity to analyze separately carrier-transport properties of electrons (minority carriers in pBp configurations) and holes (minority carriers in nBn configurations) [37,38]. We consider an nBn detector, consisting of a 50-nm-thick GaSb/AlSb superlattice barrier interposed between a 200-nm-thick InAs/GaSb absorber with a cutoff wavelength of 4.8 μm, and a top contact layer of the same superlattice.

Figure 1 shows the sub-band structure of the superlattice absorber computed with a 8×8 k · p model [3]. While, the lowest conduction sub-band (C1) shows strong dispersion along both growth (z) and in-plane (x, y) directions, the highest valence sub-band (HH1) is highly anisotropic, being actually "light" in the in-plane directions, and almost dispersion-less along the growth direction. As a preliminary step towards a computationally feasible NEGF model

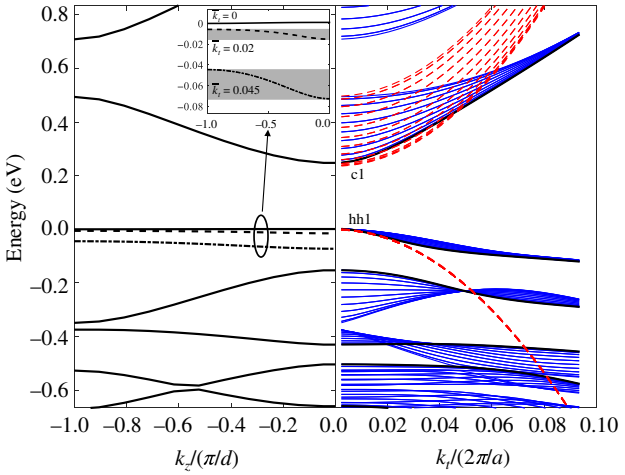

FIG. 1. Sub-band structure of a superlattice consisting in the alternating sequence of a 18/24 Å InAs/GaSb T2SL, computed with a multiband $k \cdot p$ model for wave vectors along the growth (left panel) and in-plane (right panel) directions. The in-plane dispersion for $k_z = 0$ is shown in black, while the blue curves are for equally spaced values of k_z up to the mini-Brillouin-zone boundary π/d (d is the superlattice period). Luttinger parameters are from Ref. [36]. The dashed red lines are the sub-bands computed in the effective mass approximation. The inset in the left panel shows the first heavy-hole (HH1) sub-band dispersion along k_z for different values of the (normalized) transverse wave vector k_t; the colored strips mark the corresponding minibands.

applicable to realistic devices and compatible with the drift-diffusion framework, we proceed by approximating the electronic structure in terms of parabolic valleys. Specifically, we treat the longitudinal effective masses $m^*_{e,z}$, $m^*_{h,z}$ as fitting parameters to reproduce the position of the C1 and HH1 minibands at zero transverse momentum, which gives the effective band gap of the superlattice, and we choose the transverse effective masses $m^*_{e,t}$, $m^*_{h,t}$ so as to fit the in-plane dispersion. The effective mass approximation (red dashed lines in Fig. 1) reproduces well the $k \cdot p$ electronic structure at small wave vectors. The nonparabolicity of the C1 sub-band due to the interaction between conduction and valence bands, and the slight increase in the dispersion of the HH1 sub-band along the growth direction due to heavy-hole and light-hole mixing at intermediate values of the in-plane momentum k_t (see inset), cannot be captured by single-band models. The last feature has implications in hole transport, as discussed in Ref. [40]. We return to this point later when we discuss the hole mobility. The effective masses fitting the sub-band structure of the absorber layer are reported in Table I.

Figure 2 shows the LDOS (color maps), and the conduction- and valence-band edges E_C, E_V (blue and red thin lines) of the nBn structure, computed with the NEGF approach at a reverse bias of 0.1 V. In all NEGF simulations, we use uniform grids in real and energy space, with

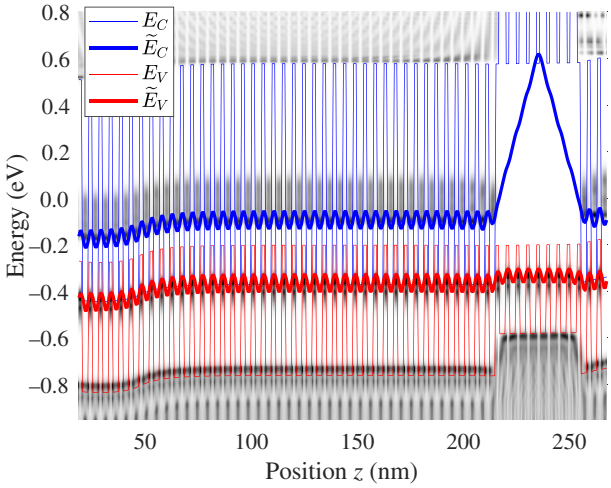

FIG. 2. Local density of states of the *n*B*n* structure, shown for zero transverse momentum. The reverse bias applied to the top (right) contact is 0.1 V. The superlattice absorber consists of 40 InAs/GaSb (18/24 Å) periods with *n*-type 10^{17} cm^{-3} doping; the same superlattice is used also for the top contact region. The doping is increased to 5×10^{18} cm^{-3} on both sides of the structure. The barrier is implemented with an undoped GaSb/AlSb (18/24 Å) superlattice to avoid the valence-band offset that typically arises when (Al, Ga)Sb is used as the barrier material [39]. The first conduction miniband of the superlattice absorber extends approximately 0.2 eV above the effective conduction-band edge $\tilde{E}_C$ (blue solid line), while the first valence miniband is strongly localized in the weakly coupled GaSb quantum wells, just below $\tilde{E}_V$ (red solid line). The band diagram (thin blue and red lines) computed with NEGF is shown for a reverse bias of 0.1 V; the SPDD band diagram (not shown for clarity) is almost superimposed to the NEGF result, save for small differences arising from the broadening effects, which are not included in the Schrödinger equation. All simulations are performed at 150 K.

steps $\Delta z = 0.5$ nm and $\Delta E = 5$ meV, respectively (the present approach is compatible with self-adaptive energy discretization techniques, see Ref. [41] for implementation details in NEMO5). The effective band edges $\tilde{E}_C$, $\tilde{E}_V$ evaluated with the SPDD model (blue and red thick lines) are computed from the corresponding carrier densities. Based on the same description of the electronic structure, SPDD and NEGF predict the same electron and hole concentrations, save for small discrepancies that can be attributed to the broadening of the states, and to a lesser extent, to energy renormalization effects, both of which are not included in the Schrödinger equation. It can be clearly seen that $\tilde{E}_C$ and $\tilde{E}_V$ mark the lower and upper borders of the first conduction and valence minibands of the superlattice absorber, respectively, meaning that they can be interpreted as landscape potentials for the corresponding carriers. In the barrier region, $\tilde{E}_C$ has a triangular shape reflecting the depleted electron density according to Eq. (22). The states in the GaSb/AlSb barrier are not visible in Fig. 2, as the energy scale has been limited to 0.5 eV (above this energy the spectral current is negligible). The different widths of the electron and hole minibands has implications on carrier transport: electron transport is mainly a coherent process through extended Bloch states, while hole transport is entirely noncoherent, meaning that the holes are strongly localized in the weakly coupled quantum wells, and their motion across the miniband is made possible by carrier-phonon scattering. The possible presence of compositional and geometrical fluctuations, not considered here, could make the difference between electron and hole mobilities even more striking [3].

Figure 3 shows the dark-current-voltage characteristics of the *n*B*n* structure computed with NEGF (circles) and SPDD (solid lines) at different temperatures. Inspection of the dark-current components reveals that the photodetector is GR limited at both temperatures. In general, barrier detectors have different dark-current contributions, including SRH generation in the depletion region, the diffusion current due to the thermal (SRH and Auger) generation of carriers in the neutral region of the absorber, intraband tunneling of the (majority) electrons across the barrier, and band-to-band tunneling (BTBT) [18]. A SRH-limited minority-carrier lifetime of 10 ns is assumed for both electrons and holes (typical values observed in InAs/GaSb T2SLs are below 100 ns, and have been attributed to native defects associated with GaSb [6]). The trap energy level is assumed at the midgap of the superlattice [42]. BTBT cannot be described within the effective mass approximation embraced in this work (see Ref. [3] for a NEGF description of interband tunneling within a multiband description of the electronic structure). However, in the voltage range explored by Fig. 3, BTBT is not expected to be relevant. Auger and radiative recombination may be included within the Büttiker-probe formalism in a similar way as SRH, but since our objective is to assess the viability of quantum-corrected approaches, we postpone this extension to a future work. A very good agreement between NEGF and SPDD results is obtained adjusting the hole mobility in the SPDD model to $\mu_h = 1$ cm^2 V^{-1} s^{-1}. Similar calculations in a dual *p*B*p* structure (obtained replacing the GaSb/AlSb electron barrier with an InAs/AlSb hole barrier) predicted an electron mobility of approximately $\mu_e = 1000$ cm^2 V^{-1} s^{-1}.

These mobilities should be interpreted as *apparent* mobilities, and they make sense only in the mathematical framework in which they are defined, in this case a drift-diffusion model with quantum corrections to account for the lowering of the barriers (tunneling effects) and the increase of energy ground states (confinement effects). The electron mobility estimated with the present approach is comparable with NEGF mobility calculations performed with a more accurate $k \cdot p$ description of the electronic structure, but limited for computational reasons to the

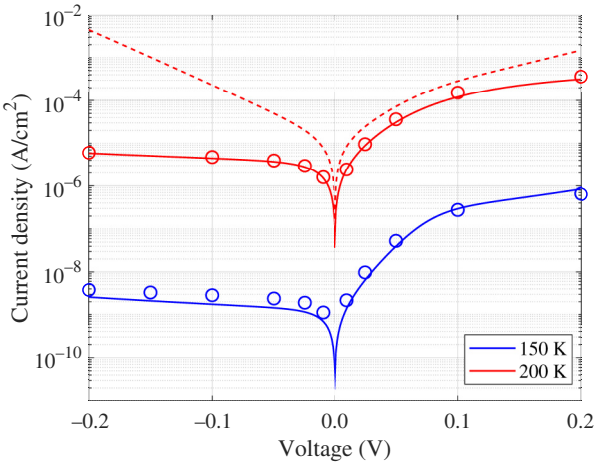

FIG. 3. Dark-current-voltage characteristics of the nBn structure computed at $T = 150$ K and $T = 200$ K, with SPDD (solid lines) and NEGF (open circles).

superlattice absorber, as discussed in Ref. [3]. On the other hand, the effective mass approximation leads to an underestimation of the hole mobility with respect to multiband NEGF calculations, which predict $\mu_h \approx 20$ cm^2 V^{-1} s^{-1}, in agreement with experimental results [43]. This difference may be traced back to the longitudinal dispersion of the HH1 miniband at intermediate transverse wave vectors induced by the mixing between heavy-hole and light-hole bands [40]. The Büttiker formalism may be extended to the multiband case, although ansatz (2) does not apply anymore. We postpone this investigation to a future work. In any case, it should be noted that the hole superlattice mobility is much smaller than the bulk mobilities of the constituent materials, which indicates that the definition of effective (bulklike) conduction- and valence-band edges does not justify the use of bulk mobility models in the hopping regime.

In a properly designed barrier detector, the flow of the majority carriers (electrons in nBn detectors) should be blocked, without impeding the flow of the minority carriers. Inspection of the dark-current contributions confirms that (intraband) electron tunneling is indeed negligible in the structure under study, as expected from the large energy separation (approximately 1 eV) between conduction minibands in the absorber and barrier layers. In the absence of tunneling of the majority carriers, part of the success of the SPDD model in reproducing NEGF I-V characteristics of barrier detectors relies in the ability to predict the correct carrier densities, from which the recombination rates follow. Less satisfactory is the capability of the SPDD model to describe the filtering properties of the barrier layer. When the width of the superlattice barrier is reduced from 50 to 25 nm, the dark current predicted by NEGF is just slightly increased, meaning that the detector performance is still limited by SRH, while the SPDD model significantly overestimates the dark current (dashed line in Fig. 3). The discrepancies between NEGF and SPDD emerging at very small barrier widths, suggest that although the qualitative behavior of tunneling is captured by SPDD through the lowering of the effective potential, the design of the barrier layer in infrared T2SL detectors may require a more rigorous analysis that only genuine quantum models can provide.

Among such models, the NEGF formalism has the additional advantage to provide spectrally resolved quantities. The spectral current computed under illumination at $T = 150$ K is shown in Fig. 4. The narrow strips following the miniband edges represent electrons and holes photogenerated in the absorber diffusing in opposite directions, the electrons to the left, the holes towards the contact layer beyond the electron barrier. The spreading of the electron spectral current in the highly doped end of the absorber is indicative of electron relaxation by phonon scattering. It is interesting to compare the Fermi levels of the Büttiker probes with the quasi-Fermi-levels computed with the SPDD model, see Fig. 4. In the barrier region, the electron Fermi levels have an error-function shape, almost steplike in the NEGF calculations, i.e., the electrons tunneling from the top contact through the barrier, rapidly become members of the absorber "ensemble," adjusting to the Fermi level on the other side of the barrier (a similar behavior can be observed in short-channel FETs [44]). In the almost field-free superlattice absorber, the NEGF and SPDD Fermi levels of the (majority) electrons are almost constant. On the other hand, the Fermi levels of the (minority) holes show a stair-case profile, which is more visible near the barrier layer, where the electric field is present. This behavior suggests that hole transport is best described

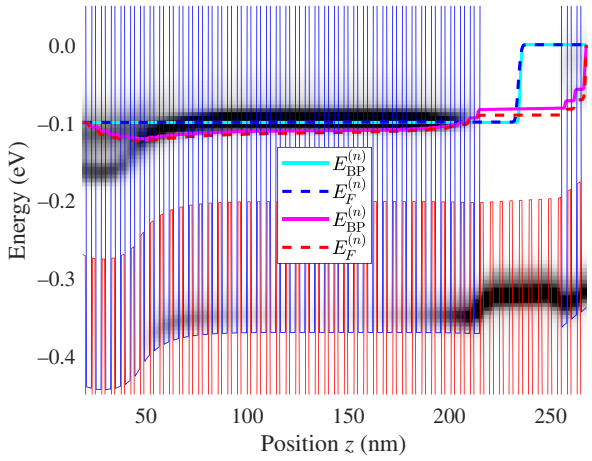

FIG. 4. Spatially and spectrally resolved current density (color maps) with a light illumination intensity of $P_{\mathrm{opt}} = 0.1$ W/m^2, and at a reverse bias of 0.1 V. The Fermi levels of the Büttiker probes (NEGF) and the quasi-Fermi-levels of the carriers (SPDD) are shown in solid and dashed lines, respectively.

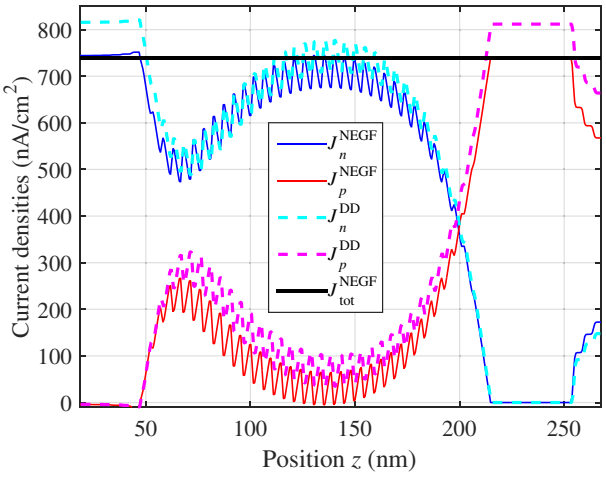

FIG. 5. Energy-integrated spatial profile of electron and hole currents obtained from NEGF (cyan and magenta solid lines), and the corresponding currents computed with the SPDD model (blue and red dashed lines). As GR processes are suppressed in the barrier (see Fig. 6), the electron and hole currents remain constant in this region. The total NEGF current (solid black line) is perfectly conserved.

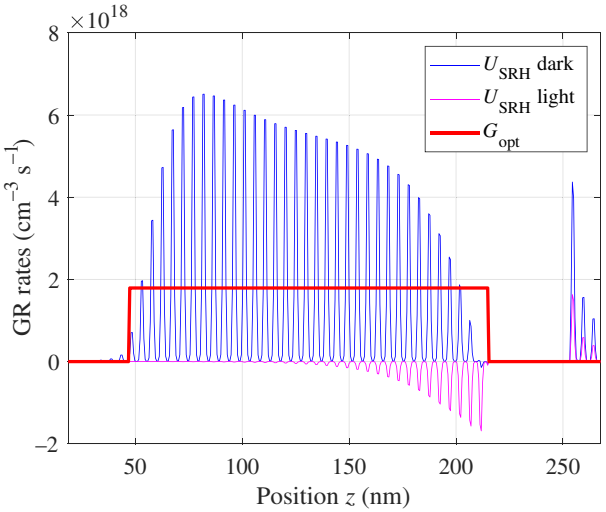

FIG. 6. Spatial profile of the SRH recombination rate in dark and illumination conditions. For simplicity, the optical generation is assumed constant in the absorbing region. The competition of SRH recombination and optical generation in the superlattice absorber is clearly visible.

by sequential tunneling, i.e., tunneling to the neighboring well followed by relaxation. These effects are captured by the SPDD model, although some small discrepancies in the Fermi levels can be noticed.

The energy-integrated electron and hole currents under illumination computed with NEGF and SPDD are compared in Fig. 5. In NEGF calculations, current conservation is achieved in just few iterations. This is perhaps the most useful advantage of the Büttiker formalism. In the superlattice absorber, the electron and hole currents have the typical shape expected in a selectively contacted device. In contrast to p-n junction photodiodes, in nBn detectors, the photogenerated holes crossing the barrier enter the contact layer as minority carriers, where they recombine at a rate governed by the carrier lifetime, prolonging the duration of the photoevent [37]. The majority carriers are effectively blocked by the barrier, as the energy-integrated electron current is virtually zero in the barrier region. The carrier extraction efficiency $\eta_{\mathrm{ext}} = J_{\mathrm{SC}}/J_{\mathrm{gen}}$ defined as the ratio between the short-circuit current J_{SC} and the generation current $J_{\mathrm{gen}} = e\int dz\, G_{\mathrm{opt}}(z)$ is found to be limited to 25% by the short diffusion length of the holes. Finally, the spatial profile of the SRH recombination rate computed in dark and in illumination conditions confirms that SRH generation is mostly limited to the depletion region on the left side of the electron barrier, see Fig. 6. Trap-assisted tunneling (TAT) is already included in both NEGF and SPDD formulations. Field-enhancement factors, which are introduced in the expression of the SRH rate to account for the presence of the tail states that participate to the recombination process [45], are not needed here, since this effect is already included in the quantum charge densities used in Eq. (13).

IV. CONCLUSION

In conclusion, NEGF calculations can be approximately reproduced by the SPDD model by correcting the LDOS with a Schrödinger solver and extracting carrier mobilities from NEGF calculations. The evaluation of critical figures of merit of infrared T2SL detectors, such as interpixel crosstalk and the modulation transfer function (MTF), requires three-dimensional simulations to model lateral diffusion from the pixel corners and neighboring pixel interactions. In particular, the MTF is sensitive to the mobility anisotropy (the hole mobility is much larger along the in-plane direction than the growth direction), which directly impacts detector performance [46]. These effects are clearly beyond the grasp of NEGF approaches. The effective semiclassical confining potentials $\tilde{E}_C$ and $\tilde{E}_V$ seen by the carriers can be efficiently computed from LL approaches. Recent LL calculations of carrier transport in nitride-based LEDs showed that the LL theory captures quantum localization and tunneling effects in disordered systems [47]. In T2SL barrier detectors, the precise evaluation of the local density of tail states is critical to evaluate sequential tunneling processes, TAT, and intraband tunneling of the majority carriers across the barrier. The accuracy of LL approaches in reproducing carrier densities and tunneling probabilities should be carefully tested before three-dimensional quantum-corrected DD simulations of T2SL detectors may be attempted.

ACKNOWLEDGMENTS

We thank Dr. Jonathan Schuster for useful discussions. This work is supported by the U.S. Army Research Laboratory through the Collaborative Research Alliance (CRA) for MultiScale multidisciplinary Modeling of Electronic materials (MSME). The computational resources are provided by the DoD HPC Systems and the 2019 Army Research Office DURIP Award (Grant No. W911NF-19-1-0161) made to Dr. E. Bellotti.

[1] D. Z.-Y. Ting, A. Soibel, L. Höglund, J. Nguyen, C. J. Hill, A. Khoshakhlagh, and S. D. Gunapala, in *Advances in infrared photodetectors*, ser. Semiconductors and semimetals. San Diego: Academic Press, 2011, ch. 1, p. 1.

[2] A. Wacker, Semiconductor superlattices: A model system for nonlinear transport, Phys. Rep. **357**, 1 (2002).

[3] F. Bertazzi, A. Tibaldi, M. Goano, J. A. Gonzalez Montoya, and E. Bellotti, Nonequilibrium Green's Function Modeling of type-II Superlattice Detectors and its Connection to Semiclassical Approaches, Phys. Rev. Appl. **14**, 014083 (2020).

[4] D. Z.-Y. Ting, A. Soibel, A. Khoshakhlagh, S. A. Keo, A. M. Fisher, S. B. Rafol, L. Höglund, C. J. Hill, B. J. Pepper, and S. D. Gunapala, Long wavelength InAs/InAsSb superlattice barrier infrared detectors with p-type absorber quantum efficiency enhancement, Appl. Phys. Lett. **118**, 133503 (2021).

[5] B. V. Olson, J. F. Klem, E. A. Kadlec, J. K. Kim, M. D. Goldflam, S. D. Hawkins, A. Tauke-Pedretti, W. T. Coon, T. R. Fortune, E. A. Shaner, and M. E. Flatté, Vertical Hole Transport and Carrier Localization in InAs/$InAs_{1-x}Sb_x$ type-II Superlattice Heterojunction Bipolar Transistors, Phys. Rev. Appl. **7**, 024016 (2017).

[6] A. Rogalski, P. Martyniuk, and M. Kopytko, InAs/GaSb type-II superlattice infrared detectors: Future prospect, Appl. Phys. Rev. **4**, 031304 (2017).

[7] M. Grupen and K. Hess, Simulation of carrier transport and nonlinearities in quantum-well laser diodes, IEEE J. Quantum Electron. **34**, 120 (1998).

[8] C. de Falco, E. Gatti, A. L. Lacaita, and R. Sacco, Quantum-corrected drift-diffusion models for transport in semiconductor devices, J. Comp. Phys. **204**, 533 (2005).

[9] B. Witzigmann, A. Witzig, and W. Fichtner, A multidimensional laser simulator for edge-emitters including quantum carrier capture, IEEE Trans. Electron Devices **47**, 1926 (2000).

[10] M. G. Ancona and A. Svizhenko, Density-gradient theory of tunneling: Physics and verification in one dimension, J. Appl. Phys. **104**, 073726 (2008).

[11] A. Tibaldi, F. Bertazzi, M. Goano, R. Michalzik, and P. Debernardi, VENUS: A vertical-cavity surface-emitting laser electro-opto-thermal numerical simulator, IEEE J. Select. Topics Quantum Electron. **25**, 1500212 (2019).

[12] D. N. Arnold, G. David, D. Jerison, S. Mayboroda, and M. Filoche, Effective Confining Potential of Quantum States in Disordered Media, Phys. Rev. Lett. **116**, 056602 (2016).

[13] M. Filoche, M. Piccardo, Y. Wu, C. Li, C. Weisbuch, and S. Mayboroda, Localization landscape theory of disorder in semiconductors. I. Theory and modeling, Phys. Rev. B **95**, 144204 (2017).

[14] M. Filoche and S. Mayboroda, Universal mechanism for Anderson and weak localization, Proc. Natl. Acad. Sci. U.S.A. **109**, 14761 (2012).

[15] T.-Y. Tsai, K. Michalczewski, P. Martyniuk, C.-H. Wu, and Y.-R. Wu, Application of localization landscape theory and the k.p model for direct modeling of carrier transport in a type II superlattice InAs/InAsSb photoconductor system, J. Appl. Phys. **127**, 033104 (2020).

[16] C. Weisbuch, S. Nakamura, Y. Wu, and J. S. Speck, Disorder effects in nitride semiconductors: Impact on fundamental and device properties, Nanophoton **10**, 3 (2021).

[17] K. Wang, R. Grassi, Y. Chu, S. H. Sureshbabu, J. Geng, P. Sarangapani, X. Guo, M. Townsend, and T. Kubis, Introduction of multi-particle Büttiker probes–bridging the gap between drift-diffusion and quantum transport, J. Appl. Phys. **128**, 014302 (2020).

[18] P. Martyniuk, M. Kopytko, and A. Rogalski, Barrier infrared detectors, Opto-Electron. Rev. **22**, 127 (2014).

[19] P. Greck, S. Birner, B. Huber, and P. Vogl, Efficient method for the calculation of dissipative quantum transport in quantum cascade lasers, Opt. Express **23**, 6587 (2015).

[20] U. Aeberhard, Quantum-kinetic theory of photocurrent generation via direct and phonon-mediated optical transitions, Phys. Rev. B **84**, 035454 (2011).

[21] T. Kubis and P. Vogl, Assessment of approximations in nonequilibrium Green's function theory, Phys. Rev. B **83**, 195304 (2011).

[22] M. Büttiker, Four-Terminal Phase-Coherent Conductance, Phys. Rev. Lett. **57**, 1761 (1986).

[23] S. Datta, Nanoscale device modeling: The Green's function method, Superlatt. Microstruct. **28**, 253 (2000).

[24] R. Venugopal, M. Paulsson, S. Goasguen, S. Datta, and M. S. Lundstrom, A simple quantum mechanical treatment of scattering in nanoscale transistors, J. Appl. Phys. **93**, 5613 (2003).

[25] J. A. Vaitkus and J. H. Cole, Büttiker probes and the recursive Green's function: An efficient approach to include dissipation in general configurations, Phys. Rev. B **23**, 085149 (2018).

[26] S.-C. Lee and A. Wacker, Nonequilibrium Green's function theory for transport and gain properties of quantum cascade structures, Phys. Rev. B **66**, 245314 (2002).

[27] A. Wacker, M. Lindskog, and D. O. Winge, Nonequilibrium Green's function model for simulation of quantum cascade laser devices under operating conditions, IEEE J. Select. Topics Quantum Electron. **19**, 1200611 (2013).

[28] T. Schmielau and M. F. Pereira, Impact of momentum dependent matrix elements on scattering effects in quantum cascade lasers, Phys. Status Solidi B **246**, 329 (2009).

[29] U. Aeberhard, Challenges in the NEGF simulation of quantum-well photovoltaics posed by non-locality and localization, Phys. Status Solidi B **99**, 1800500 (2019).

[30] P. Sarangapani, Y. Chu, J. Charles, G. Klimeck, and T. Kubis, Band-Tail Formation and Band-Gap Narrowing Driven by Polar Optical Phonons and Charged Impurities

in Atomically Resolved III-V Semiconductors and Nanodevices, Phys. Rev. Appl. **12**, 044045 (2019).

[31] J. S. Blakemore, Approximation for Fermi-Dirac integrals, especially the function $\mathcal{F}_{\frac{1}{2}}(\eta)$ used to describe electron density in a semiconductor, Solid-State Electron. **25**, 1067 (1982).

[32] M. Goano, Series expansion of the Fermi-Dirac integral $\mathcal{F}_j(x)$ over the entire domain of real j and x, Solid-State Electron. **36**, 217 (1993).

[33] U. Aeberhard, Nonequilibrium Green's function picture of nonradiative recombination of the Shockley-Read-Hall type, Phys. Rev. B **99**, 125302 (2019).

[34] K. Wang, Y. Chu, D. Valencia, J. Geng, J. Charles, P. Sarangapani, and T. Kubis, in *International Conference on Simulation of Semiconductor Processes and Devices (SISPAD 2018)*, 2018, p. 5.

[35] *Sentaurus Device User Guide. Version F-2011.09*, Synopsys, Inc., Mountain View, CA, Sept. 2011.

[36] P. C. Klipstein, Y. Livneh, A. Glozman, S. Grossman, O. Klin, N. Snapi, and E. Weiss, Modeling InAs/GaSb and InAs/InAsSb superlattice infrared detectors, J. Electron. Mater. **43**, 2984 (2014).

[37] M. Reine, J. Schuster, B. Pinkie, and E. Bellotti, Numerical simulation and analytical modeling of InAs nBn infrared detectors with p-type barriers, J. Electron. Mater. **42**, 3015 (2013).

[38] M. Reine, B. Pinkie, J. Schuster, and E. Bellotti, Numerical simulation and analytical modeling of InAs nBn infrared detectors with n-type barriers, J. Electron. Mater. **43**, 2915 (2014).

[39] A. Jang, H. J. Lee, Y. H. Kim, H. Jung, P. Bidenko, and S. Kim, in *2021 International Conference on Electronics, Information, and Communication (ICEIC)*, Feb. 2021, p. 20431923.

[40] D. Z. Y. Ting, A. Soibel, L. Höglund, and S. D. Gunapala, Theoretical aspects of minority carrier extraction in unipolar barrier infrared detectors, J. Electron. Mater. **44**, 3036 (2015).

[41] J. Charles, P. Sarangapani, R. Golizadeh-Mojarad, R. Andrawis, D. Lemus, X. Guo, D. Mejia, J. E. Fonseca, M. Povolotskyi, T. Kubis, and G. Klimeck, Incoherent transport in NEMO5: Realistic and efficient scattering on phonons, J. Comp. Electron. **15**, 1123 (2016).

[42] Y. Aytac, B. V. Olson, J. K. Kim, E. A. Shaner, S. D. Hawkins, J. F. Klem, M. E. Flatté, and T. F. Boggess, Temperature-dependent optical measurements of the dominant recombination mechanisms in InAs/InAsSb type-2 superlattices, J. Appl. Phys. **118**, 125701 (2015).

[43] P. C. Klipstein *et al.*, in *Proc. SPIE 11741*, Apr. 2021, p. 117410N.

[44] A. Schenk, P.Aguirre, TCAD models of the ballistic mobility in the source-to-drain tunneling regime, Solid-State Electron. **157**, 1 (2019).

[45] G. A. M. Hurkx, D. B. M. Klaassen, and M. P. G. Knuvers, A new recombination model for device simulation including tunneling, IEEE Trans. Electron Devices **39**, 331 (1992).

[46] J. Schuster, Assessment of the modulation transfer function in infrared detectors with anisotropic material properties: Type-II superlattices, IEEE Trans. Electron Devices **66**, 1338 (2019).

[47] C.-K. Li, M. Piccardo, L.-S. Lu, S. Mayboroda, L. Martinelli, J. Peretti, J. S. Speck, C. Weisbuch, M. Filoche, and Y.-R. Wu, Localization landscape theory of disorder in semiconductors. III. application to carrier transport and recombination in light emitting diodes, Phys. Rev. B **95**, 144206 (2017).